

Investigating Orbital Magnetic Moments in Spinel-Type MnV_2O_4 Using X-ray Magnetic Circular Dichroism

Jun Okabayashi^{1*}, Shigeki Miyasaka², Kazuhiro Hemmi², Kiyohisa Tanaka^{2,3}, Setsuko Tajima², Hiroki Wadati⁴, Arata Tanaka⁵, Yasumasa Takagi³, and Toshihiko Yokoyama³

¹Research Center for Spectrochemistry, University of Tokyo, Bunkyo, Tokyo 113-0033, Japan

²Department of Physics, Osaka University, Toyonaka, Osaka 560-0043, Japan

³Institute for Molecular Science, Okazaki, Aichi 444-8585, Japan

⁴Institute for Solid State Physics, University of Tokyo, Kashiwa, Chiba 227-8581, Japan

⁵Department of Quantum Matter, Hiroshima University, Higashihiroshima, Hiroshima 739-8530, Japan

(Received March 13, 2015; accepted July 23, 2015; published online September 7, 2015)

Element-specific magnetic structures, particularly orbital magnetic moments, of spinel-type MnV_2O_4 were investigated using X-ray magnetic circular dichroism (XMCD). X-ray absorption and XMCD spectra clearly reveal that the Mn^{2+} (d^5) and V^{3+} (d^2) states are coupled antiferromagnetically. Analyses of XMCD spectra using magneto optical sum rules revealed that small but finite orbital magnetic moments remain in both V and Mn $3d$ states, which accounts for the antiferro-type orbital ordering in the V sites of MnV_2O_4 with coexisting complex and real orbital states. Additionally, the Cr doping effect in MnV_2O_4 was examined. The XMCD spectra of Cr^{3+} (d^3) L -edges exhibited the substitution of Cr ions to the V sites ferromagnetically, with low conductivity through the suppression of the orbital ordering.

1. Introduction

Couplings between orbital and spin degrees of freedom in transition metal (TM) oxides exhibit a wide variety of interesting physical phenomena studied in strongly correlated electron systems.¹ The orbital degeneracy of t_{2g} or e_g orbitals, split by the crystal field in TM oxides, gives rise to the orbital ordering phenomena in perovskite-type Mn or V oxides accompanied by Jahn–Teller distortion.^{2,3} Spinel-type vanadium oxides (AV_2O_4) are one of the candidates used to investigate the orbital ordering phenomena using charge, spin, and orbital degrees of freedom. These materials have attracted considerable attention owing to the topologically frustrated pyrochlore lattices of V atoms, which induce orbital ordering through structural transition from cubic to tetragonal symmetries. The orbital degeneracy of d^2 systems in octahedrally coordinated TM $3d$ t_{2g} orbitals allows for the controllability of orbital states through local lattice distortion. Interesting physics in the long-range orbital ordering using the Jahn–Teller active d^2 electrons in V^{3+} states has been extensively investigated for AV_2O_4 (A: Zn, Cd, Mg),^{4–6} MnV_2O_4 ,^{7–11} and FeV_2O_4 .^{12,13} MnV_2O_4 is a good candidate for studying orbital ordering since the orbital magnetic moments of Mn^{2+} (d^5) are nearly quenched with relatively large spin moments in high spin states. Extensive studies of orbital ordering in MnV_2O_4 have been performed using X-ray diffraction,¹⁴ neutron diffraction,^{15,16} optical conductivity,¹⁷ Raman spectroscopy,¹⁸ nuclear magnetic resonance of ^{51}V ,¹⁹ and first-principles calculations.^{20,21} X-ray diffraction using synchrotron radiation shows that the structural transition from cubic $Fd\bar{3}m$ to tetragonal $I4_1/a$ symmetry occurs as the temperature decreases from the spin transition temperature above 59 K to the orbital ordering temperature below 54 K.¹⁴ On the basis of neutron scattering, the total (spin and orbital) magnetic moments of Mn and V atoms were estimated to be 4.2 and $1.3 \mu_B$, respectively,¹⁵ although the spin and orbital components were not distinguished. In addition, functional properties such as magneto caloric effects and magnetic shape memory effects in MnV_2O_4 were also

demonstrated in the interval temperature between spin and orbital orderings.^{22,23}

An unresolved issue related to the orbital ordering of spinel-type vanadium oxides is the relationship between the orbital magnetic moments in vanadium sites and the orbital ordering. In particular, the type of orbital ordering that occurs has been under dispute. One type is the antiferro-orbital ordering with alternate occupations of yz and zx along the c -axis proposed by Motome and Tsunetsugu,²⁴ which results in the space group $I4_1/a$ and the real wave functions d_{yz}/d_{zx} due to the quenching of orbital angular momentums. The presence of this type of ordering suggests that the spin–orbit interactions in V $3d$ states are negligible. The other type is the ferro-orbital ordering with occupied degenerated orbitals proposed by Tchernyshyov,²⁵ shown as $d_{yz} + id_{zx}$, which results in complex wave functions of the space group $I4_1/amd$ symmetry. Large orbital moments are expected with this type of ordering. In order to determine the type of orbital ordering in MnV_2O_4 , element-specific and quantitative measurements of orbital magnetic moments are essential. Although the spin magnetic moments summing the antiparallel coupling between Mn^{2+} (d^5 , $S = 5/2$) and V^{3+} (d^2 , $S = 1$) were estimated from magnetization measurements,¹⁰ the element-specific orbital magnetic moments of each ion have not been investigated. Additionally, $I4_1/amd$ complex wave functions are considered to occur in FeV_2O_4 because the tetrahedral coordinated high-spin d^6 systems in Fe sites involve the doubly degenerate e states with orbital ordering.¹⁴ The Orbital-Peierls model with the space group $P4_12_12$ was also proposed by Khomskii and Mizokawa²⁶ for related spinel-type compounds, although this model does not exhibit the mirror, glide, and face-centered symmetries of the spinel structure. First-principles calculations for MnV_2O_4 predict collinear orbital chains along the V sites in a pyrochlore lattice.^{20,21} Sarkar et al. proposed that the large trigonal distortion in the VO_6 octahedra modulates the orbital ordering type.²⁰ Local density approximations (LDAs) including the intra-atomic Coulomb interaction (U) and spin–orbit interaction reveal that the mixing states of the real

and complex wave functions are essential for the ground-state configurations.²⁰⁾ Strong exchange interactions between the V sites and the large U values are expected with complex orbital ordering. The Coulomb-enhanced spin-orbit effects are also candidates for the generation of orbital magnetic moments.²⁰⁾ Optical conductivity measurements¹⁷⁾ using multiplet spectral analysis suggest the mixing of real and complex orbital orderings. Therefore, the investigation of element-specific orbital magnetic moments in MnV_2O_4 is strongly desired in order to clarify the physics behind the orbital ordering phenomena.

X-ray magnetic circular dichroism (XMCD) with X-ray absorption spectroscopy (XAS) using polarized synchrotron radiation is a powerful technique for investigating the magnetic and electronic states, particularly element-specific spin and orbital moments. The analysis of XMCD using magneto optical sum rules enables us to deduce the precise orbital magnetic moments.²⁷⁾ The spin sum rules are not applicable to spin magnetic moments in early $3d$ TMs owing to the failure of the separation of core-hole spin-orbit interactions and the existence of magnetic dipole terms.²⁸⁾ These rules are applicable empirically only for the late $3d$ TMs such as Mn, Fe, Co, and Ni compounds. On the other hand, for orbital magnetic moments, the orbital sum rule is in principle applicable even in vanadium compounds because the overlap between the core-hole spin-orbit splitting cancels out in the orbital sum rule analysis. For the analysis of XAS and XMCD spectra, the cluster-model simulation including the configuration interaction (CI) approach was used to determine the electronic structure parameters accompanied by spin and orbital magnetic moments. We employed not only sum rules but also cluster-model calculations with CI, which are suitable for deducing the electronic structure parameters and spin and orbital magnetic moments.

Recently, Hemmi et al.¹¹⁾ reported that Cr or Mo impurities in MnV_2O_4 suppressed the orbital ordering owing to the t_{2g} orbitals being fully occupied. We examined if the Cr^{3+} or Mo^{3+} impurities (d^3) substituted the V^{3+} sites with additional electron numbers, resulting in metallic conductivity. We found that the critical temperature for orbital ordering decreased from 59 to 40 K after 13% Cr doping, suggesting that orbital ordering occurred in V^{3+} ions. However, the spin configurations of each element need to be determined explicitly. Investigations of the effects of impurity doping on element-specific magnetic moments enable us to discuss the modulation of orbital ordering.

In this study, we investigated the element-specific electronic and magnetic properties of MnV_2O_4 using XAS and XMCD, and examined the relationship between orbital magnetic moments and orbital ordering. We employed magneto optical sum rules and cluster-model calculations for the analysis of XMCD to deduce the orbital magnetic moments. We found that the finite orbital magnetic moments in V sites contribute to the orbital ordering type through the mixing of real and complex wave functions. Furthermore, we examined the Cr doping effect in MnV_2O_4 using XMCD.

2. Methods

Polycrystalline samples of MnV_2O_4 were synthesized by a solid-state reaction method. Single crystals were grown from the polycrystalline samples by the floating-zone method.

Details of the sample preparation and the fundamental physical properties are provided in Ref. 11. The magnetic and orbital ordering temperatures of MnV_2O_4 were estimated to be 59 and 54 K, respectively. The XAS and XMCD measurements were performed at BL-4B, UVSOR, Institute of Molecular Science, Japan. The XAS spectra with different helicities were obtained by switching the magnetic fields in the parallel and antiparallel directions along the incident beam. The total photoelectron yield mode by directly detecting the sample current was adopted. The extent of circular polarization (P) was evaluated to be $71 \pm 0.5\%$. The photon energy resolution was set at 100 meV. The XAS and XMCD measurements were performed at a sample temperature of 5 K. A magnetic field of ± 5 T, produced using a superconducting magnet, was applied in the direction of the incident polarized soft X-ray.²⁹⁾ MnV_2O_4 rods were scraped into a powder in air prior to the XAS and XMCD measurements, in order to prevent the charge-up effect during the photoelectron emission process. Since the probing depth of photoelectrons was approximately 5 nm in the TM L -edge photon energy regions, some contamination on the surfaces was expected in the oxygen K -edge XAS spectrum. However, we could assume that the XMCD signals were derived from the intrinsic magnetic properties of MnV_2O_4 from the XAS line shapes of both Mn and V L -edges.

3. Results and Discussion

Figure 1(a) shows XAS, XMCD, and the integrated XMCD spectra of V $L_{2,3}$ -edge regions taken at 5 K, which is sufficiently lower than the orbital ordered transition temperature. Comparing the XAS line shapes with reference line shapes in vanadium oxides possessing other valence states such as V_2O_3 , VO_2 , and V_2O_5 ,^{30,31)} we infer from the XAS spectra that V^{3+} states are formed. Several fine structures were observed in the V L -edge XAS spectrum, and clear differences depending on the magnetic field, i.e., photon helicities, were observed in the XMCD signals. The XMCD intensities were estimated to be approximately 5% of the XAS intensities at the L_3 main peak of 518 eV depending on the helicities of σ^+ and σ^- . The complicated XMCD signals were derived from the final-state multiplet structures of V^{3+} ions. In previous studies of V^{3+} states, using XMCD, in FeV_2O_4 measured at 80 K, similar complicated line shapes of both XAS and XMCD have been observed.³²⁾ Although spin sum rules cannot be adopted for the V L -edge XMCD because of the small spin-orbit splitting of V $L_{2,3}$ edges,²⁸⁾ asymmetric intensities in the XMCD spectra between V L_2 and L_3 edges can be evaluated by the integration of XMCD spectra. The orbital sum rule for XMCD spectral analysis implies that the orbital magnetic moments are proportional to the integrals of XMCD signals along $L_{2,3}$ edges and the $3d$ electron numbers.²⁷⁾ The positive and negative asymmetric XMCD signals at L_3 and L_2 edges, respectively, can be observed in Fig. 1(a). The resulting residuals (q) from the XMCD integrals for both L_2 and L_3 edges are shown at the bottom of Fig. 1(a), suggesting that the finite values of orbital magnetic moments remained in the V^{3+} states. The integral of XAS ($\sigma^+ + \sigma^-$) after subtracting the background is also shown in the third panel of Fig. 1. Using the integrals over XAS spectra (r) and assuming that the V $3d$ electron number

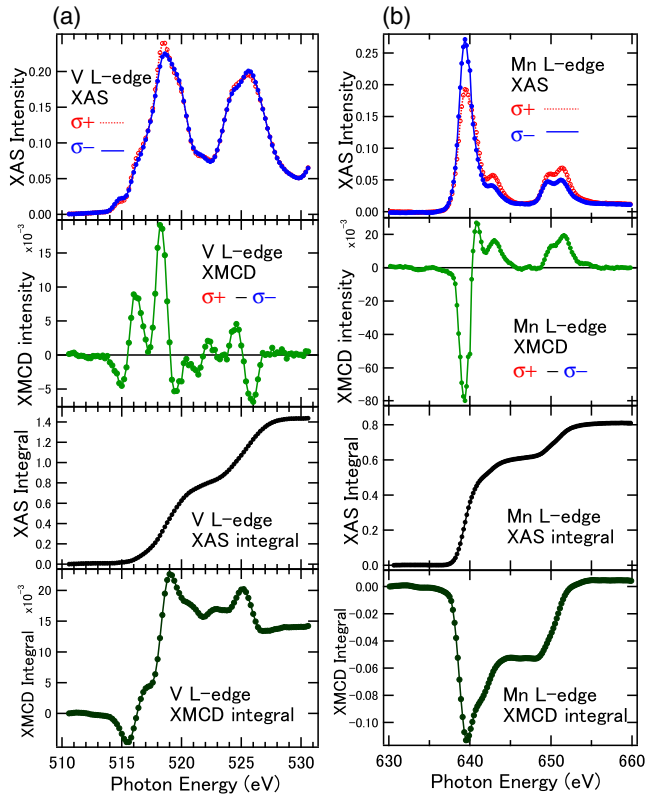


Fig. 1. (Color online) XAS, XMCD, and their integrated spectra in MnV_2O_4 for (a) V and (b) Mn L -edges at a temperature of 5 K and magnetic field of ± 5 T. σ^+ and σ^- denote the helicities depending on the magnetic field direction.

(n_e) is 2 ± 0.2 , we deduced the orbital magnetic moments (m_{orb}) in the expression of the orbital sum rule:³³⁾

$$m_{\text{orb}} = \frac{1}{P} \frac{4q}{3r} (10 - n_e).$$

m_{orb} is deduced to be $0.150 \pm 0.023 \mu_{\text{B}}/(\text{V atoms})$ from the orbital sum rule. The finite m_{orb} indicates that unquenched orbital magnetic moments contribute to complex wave functions in V sites. The physical origins of the finite but small amplitudes of the orbital magnetic moments in V sites are discussed below.

Mn $L_{2,3}$ -edge XAS and XMCD spectra are also shown in Fig. 1(b). The XAS spectral line shapes with multiplet structures are similar to those of Mn^{2+} compounds with T_d symmetry such as (Ga, Mn)As ferromagnetic semiconductors in the tetrahedral Mn^{2+} situations.³⁴⁾ The XMCD intensities in Fig. 1(b) were estimated to be approximately 23% at the L_3 -edge main peak of 639 eV by comparison with those of XAS. The XMCD intensities of Mn $L_{2,3}$ edges are higher than those of the V $L_{2,3}$ edges. Also, the sign of the XMCD signals is opposite to that of the V L -edge XMCD signal. This clearly indicates the antiparallel coupling of total magnetic moments between Mn^{2+} and V^{3+} ions, consistent with the well-known ferrimagnetic properties of MnV_2O_4 ,¹⁰⁾ which is also analogous to the case of FeV_2O_4 .³²⁾ The integral over the XMCD spectrum along the Mn L_2 and L_3 edges converged to a small positive value, as shown in the bottom panel in Fig. 1(b), because the areas of the positive and negative intensities were almost equivalent. This suggests that the quite small orbital magnetic moments of Mn are

Table I. Spin and orbital magnetic moments of V and Mn in MnV_2O_4 estimated from the magneto optical sum rules of XMCD spectra shown in Fig. 1. The spin sum rule for V L -edge cannot be adopted. The electronic structure parameters used in the cluster-model calculations of V and Mn in MnV_2O_4 shown in Fig. 2 are also listed. Error bars are about 10% for each value.

Elements	XMCD and sum rules		Electronic structure parameters in cluster-model calculations			
	$m_{\text{spin}} [\mu_{\text{B}}]$	$m_{\text{orbital}} [\mu_{\text{B}}]$	Δ (eV)	U (eV)	$pd\sigma$ (eV)	$10Dq$ (eV)
V	—	0.150	4.0	5.0	1.7	1.0
Mn	4.17	0.058	4.0	5.0	1.5	0.0

deduced as the less-than-half 3d TM systems. Applying the spin sum rules for Mn $L_{2,3}$ -edge XMCD with the correlation factor ($C = 0.68$) of Mn^{2+} considering the L_3 and L_2 edge overlap:^{35,36)}

$$m_{\text{spin}} = \frac{1}{PC} \frac{6p - 4q}{r} (10 - n_e),$$

where p is the integral of XMCD for only the L_3 edge, we obtained $m_{\text{spin}} = 4.17 \pm 0.63 \mu_{\text{B}}/\text{Mn}$ and $m_{\text{orb}} = 0.058 \pm 0.009 \mu_{\text{B}}/\text{Mn}$, which indicates the ratio of $m_{\text{orb}}/m_{\text{spin}} = 0.013$, suggesting the quite small contribution of orbital magnetic moments because we assume a $3d^5$ configuration with $n_e = 5$. The spin and orbital magnetic moments are listed in Table I.

For the analysis of XAS and XMCD spectra, we employed cluster-model calculations including the CI for Mn^{2+} and V^{3+} sites in MnV_2O_4 as tetrahedral (T_d) MnO_4 and octahedral (O_h) VO_6 clusters, modeled as a fragment of the spinel-type structures. The Hamiltonian included the electronic structure parameters of full on-site TM $3d-3d$ (valence–valence) and $2p-3d$ (core–valence) Coulomb interactions (U) and the T_d or O_h crystal fields ($10Dq$) in the TMs, along with the hybridization between the TM $3d$ and O $2p$ wave functions. The charge-transfer energy was defined as $\Delta = E(d^{n+1}\underline{L}) - E(d^n)$, where \underline{L} denotes a hole in a ligand p orbital. The hybridization between the TM $3d$ and O $2p$ states was also parameterized in terms of the Slater–Koster parameters ($pd\sigma$) and ($pd\pi$), where the relation ($pd\pi$) = $-(pd\sigma)/2$ was used.³⁷⁾ The parameters ($pp\sigma$) and ($pp\pi$) were always set to zero. In all cases, a Gaussian broadening was used to simulate spectral broadening.

Figure 2 shows the calculated XAS and XMCD spectra of V and Mn L -edges obtained using the cluster models with CI. We assumed that the V^{3+} (d^2) states had O_h symmetry and the Mn^{2+} (d^5) states had T_d symmetry. The electronic structure parameters were chosen to reproduce the experimental results and are listed in Table I. In first-principles calculations using the LDA+ U method, the Coulomb interaction $U_{dd} = 4.5$ eV was adopted to model the orbital ordering physics.²⁰⁾ We also use similar U values for the cluster-model calculation ($U = 5$ eV). The electronic structure parameters Δ , U , $10Dq$, and ($pd\sigma$) used for the calculations are plausible parameters for spinel-type oxides. In the case of Mn ions, the cluster-model simulations reproduce the spectral line shapes of both XAS and XMCD qualitatively, as shown in Fig. 2(b). Because of the d^5 electron system in high-spin states, the orbital magnetic moments in Mn sites are almost quenched. Spin magnetic moments of approximately $4.5 \pm 0.4 \mu_{\text{B}}$ are consistent with

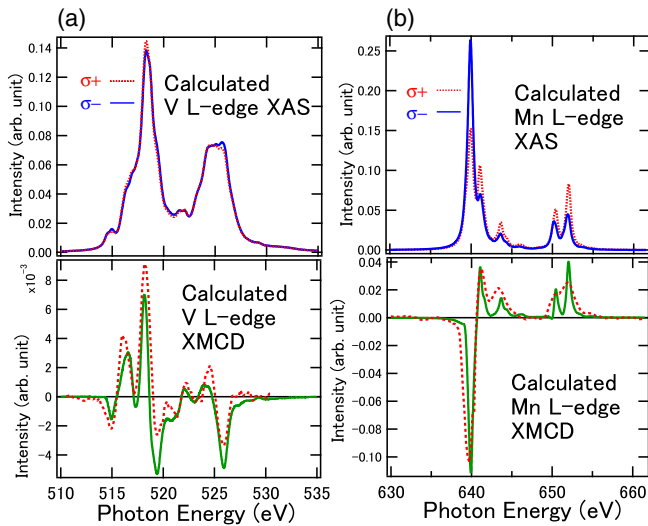


Fig. 2. (Color online) Cluster-model calculations of XAS and XMCD in MnV_2O_4 for (a) V and (b) Mn L -edges. Dot curves at the bottom panels are the experimental spectra shown in Fig. 1 for comparison.

the Mn d^5 states deduced from the XMCD analysis. The CI contributions of the ground states are estimated to be d^5 : 80.2%, $d^6\bar{L}$: 19.3%, and $d^7\bar{L}^3$: 0.02%. These results support the claim that the obtained parameters reasonably model the physical phenomena for MnV_2O_4 .

In the case of V L -edges, qualitatively similar spectral line shapes with both XAS and XMCD spectra in Fig. 1 were reproduced by the cluster-model calculation. Tetragonal local lattice distortion around the V sites must also be considered. The t_{2g} states are split into two levels by the tetragonal distortion, and the lowest xy states are occupied by one of the electrons. The other electron occupies the yz or zx states. We determined the tetragonal distortion for the V $3d$ states (D_{tet}) to be 0.02 eV in order to reproduce the complicated XMCD spectral line shapes qualitatively. The best fitted parameter sets reveal the spin magnetic moment of $1.2 \pm 0.2 \mu_B$, which is not sensitive to the electronic structure parameters. At least, the peak positions in each multiplet structure are reproduced by the calculations. Since the intensities in the calculated spectrum do not perfectly coincide with the XMCD spectrum, particularly for the L_2 and L_3 intensity ratios, the orbital magnetic moment is not deduced from the cluster-model calculation explicitly. The CI contributions of the ground states are estimated to be d^2 : 42.8%, $d^3\bar{L}$: 44.9%, $d^4\bar{L}^2$: 11.4%, and $d^5\bar{L}^3$: 0.88%. Spin-orbit interaction coefficients (λ) also become the parameters, where the nonzero value of 0.5λ is adopted for the fitting. The λ values of 0λ or 1λ have been reported in Ref. 32. Therefore, the orbital mixing of V yz and zx orbitals in MnV_2O_4 induces the small but finite orbital magnetic moments in V sites for orbital ordering.

In view of the above results, we discuss the site specific spin and orbital magnetic moments of MnV_2O_4 deduced from the XMCD analysis. By comparing the XMCD intensities between Mn and V spectra, the smaller intensities of the V L -edge XMCD compared with those of Mn reveal the spin-canted geometry in V sites, consistent with the noncollinear magnetic structures with the 2-in and 2-out spin configurations as reported in the literature. The XMCD integrals for

Mn converge to a small value while those for V remain finite. This clearly suggests the existence of the small but finite orbital magnetic moments in the V sites, which can be explained by the (i) complex orbital ordering as discussed in the case of FeV_2O_4 , (ii) domain formation, and (iii) mixing of the real and complex orbital orderings due to the trigonal distortion around the V sites. First, as reported using synchrotron radiation X-ray diffraction measurements, the complex orbital ordering is related to the high symmetry of $I4_1/amd$ in FeV_2O_4 .¹⁴⁾ The different nature of the orbital ordering between MnV_2O_4 and FeV_2O_4 is a result of the crystal symmetry. As expected in the complex orbital ordering cases, unquenched large orbital magnetic moments of $1 \mu_B$ with the spin magnetic moments of $2 \mu_B$ with the opposite sign should be anticipated. Therefore, the simple complex orbital ordering is not an acceptable model for MnV_2O_4 . Although the previous reports of XMCD in FeV_2O_4 resulted in quenched orbital magnetic moments in V sites, the measurement temperature might be far above the critical temperature for the orbital ordering, indicating the difficulty in comparing and discussing the types of orbital ordering.³²⁾ We note that in FeV_2O_4 , the high-spin d^6 configuration of Fe^{2+} ions is twofold degenerate in e orbitals resulting in unquenched orbital moments, which trigger further complex orbital ordering when combined with V ions resulting in physical properties different from those of MnV_2O_4 . Second, since the samples were scraped to powder, for the XMCD measurements, some domains might be introduced. However, the reasonable values of spin and orbital magnetic moments of Mn guarantee to clarify the physics from the obtained XMCD spectra. Therefore, the scenario of the domain formation is a minor effect. Third, the theoretical calculations and some experiments fail to suggest a simple real orbital ordering scenario in MnV_2O_4 .^{15,19,20)} Although the crystal symmetry of MnV_2O_4 possesses the $I4_1/a$, the trigonal distortion in VO_6 octahedra modulates the orbital ordering. Therefore, the finite orbital magnetic moments deduced from XMCD analysis can be explained as the mixing of real and complex orbital orderings. As an element-specific direct observation of orbital ordering, ^{51}V NMR measurements become comparable for the discussion.¹⁹⁾ It also supports the antiferro-type orbital ordering with a small amount of the ferro-type one through the local lattice distortion, although the $I4_1/a$ space symmetry of the antiferro-type one is maintained. The small but finite orbital magnetic moments in V sites deduced from XMCD measurements are consistent with the theoretical proposal by Sarkar et al.²⁰⁾ and other experiments,¹⁷⁾ that is, the mixing of real and complex orbital orderings is essential for the orbital ordering picture in MnV_2O_4 .

Finally, we discuss the effects of Cr doping in MnV_2O_4 . Figure 3 shows the Cr L -edge XAS and XMCD spectra for 13% Cr doped MnV_2O_4 . Clear XMCD signals were observed with a positive sign at the L_3 edge and a negative sign at the L_2 edge, which is the same sign direction as that for the V XMCD spectra. The XAS spectral line shapes in comparison with the XAS spectra of other Cr compounds indicated that Cr^{3+} ($3d^3$) states were formed.³⁸⁾ These results suggest that the Cr ions shift to V sites with 3+ valence states and are coupled ferromagnetically with V ions. We note that the XAS and XMCD line shapes of Mn and V L -edges remain

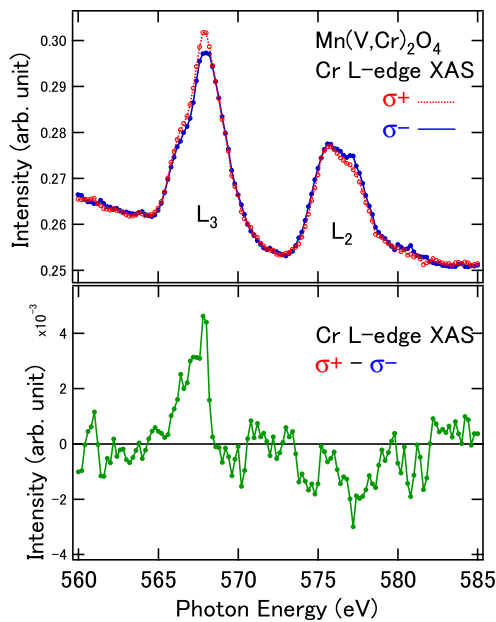


Fig. 3. (Color online) XAS and XMCD spectra of the Cr *L*-edges in 13% Cr-doped MnV_2O_4 .

unchanged (not shown). The Cr^{3+} states can explain the suppression of orbital ordering temperature because $3d^3$ electrons in Cr^{3+} states fully occupy the t_{2g} states and the orbital degree of freedom is quenched.

4. Summary

We investigated element-specific magnetic structures of spinel-type MnV_2O_4 using XMCD. X-ray absorption and XMCD spectra along with theoretical cluster-model analysis clearly revealed that Mn^{2+} (d^5) and V^{3+} (d^2) states are coupled antiferromagnetically. Analysis of XMCD spectra using sum rules revealed that small but finite orbital magnetic moments remain in V $3d$ states, indicating that the complex and real orbital ordered states coexist. Furthermore, the Cr *L*-edge XMCD revealed that the Cr doping in MnV_2O_4 enabled the substitution of the V site with the same spin direction.

Acknowledgements

This work was performed under the approval of the UVSOR facility programs at the Institute of Molecular Science, Japan. This work was partly supported by the Nanotechnology Platform Program (Molecule and Material Synthesis). We thank Professor Takashi Mizokawa (Waseda University) for fruitful discussion.

*jun@chem.s.u-tokyo.ac.jp

- 1) M. Imada, A. Fujimori, and Y. Tokura, *Rev. Mod. Phys.* **70**, 1039 (1998).
- 2) Y. Tokura and N. Nagaosa, *Science* **288**, 462 (2000).
- 3) S. Miyasaka, T. Okuda, and Y. Tokura, *Phys. Rev. Lett.* **85**, 5388 (2000).
- 4) T. Maitra and R. Valenti, *Phys. Rev. Lett.* **99**, 126401 (2007).
- 5) N. Nishiguchi and M. Onda, *J. Phys.: Condens. Matter* **14**, L551

- (2002).
- 6) E. M. Wheeler, B. Lake, A. T. M. Nazmul Islam, M. Reehuis, P. Steffens, T. Guidi, and A. H. Hill, *Phys. Rev. B* **82**, 140406(R) (2010).
- 7) R. Plumier and M. Sougi, *Physica B* **155**, 315 (1989).
- 8) K. Myung-Whun, J. S. Kim, T. Katsufuji, and R. K. Kremer, *Phys. Rev. B* **83**, 024403 (2011).
- 9) K. Adachi, T. Suzuki, K. Kato, K. Osaka, M. Takata, and T. Katsufuji, *Phys. Rev. Lett.* **95**, 197202 (2005).
- 10) T. Suzuki, M. Katsumura, K. Taniguchi, T. Arima, and T. Katsufuji, *Phys. Rev. Lett.* **98**, 127203 (2007).
- 11) K. Hemmi, R. Fukuta, E. Uykur, S. Miyasaka, S. Tajima, A. Nakao, H. Nakao, R. Kumai, and Y. Murakami, *J. Phys. Soc. Jpn.* **81**, SB030 (2012).
- 12) T. Katsufuji, T. Suzuki, H. Takei, M. Shingu, K. Kato, K. Osaka, M. Takata, H. Sagayama, and T. Arima, *J. Phys. Soc. Jpn.* **77**, 053708 (2008).
- 13) S. Nishihara, W. Doi, H. Ishibashi, Y. Husokoshi, X.-M. Ren, and S. Mori, *J. Appl. Phys.* **107**, 09A504 (2010).
- 14) Y. Nii, H. Sagayama, T. Arima, S. Aoyagi, R. Sakai, S. Maki, E. Nishibori, H. Sawa, K. Sugimoto, H. Ohsumi, and M. Takata, *Phys. Rev. B* **86**, 125142 (2012).
- 15) V. O. Garlea, R. Jin, D. Mandrus, B. Roessli, Q. Huang, M. Miller, A. J. Schultz, and S. E. Nagler, *Phys. Rev. Lett.* **100**, 066404 (2008).
- 16) J.-H. Chung, J.-H. Kim, S.-H. Lee, T. J. Sato, T. Suzuki, M. Katsumura, and T. Katsufuji, *Phys. Rev. B* **77**, 054412 (2008).
- 17) T. Katsufuji, T. Takubo, and T. Suzuki, *Phys. Rev. B* **87**, 054424 (2013).
- 18) K. Takubo, R. Kubota, T. Suzuki, T. Kanzaki, S. Miyahara, N. Furukawa, and T. Katsufuji, *Phys. Rev. B* **84**, 094406 (2011).
- 19) S.-H. Baek, N. J. Curro, K.-Y. Choi, A. P. Reyes, P. L. Kuhns, H. D. Zhou, and C. R. Wiebe, *Phys. Rev. B* **80**, 140406(R) (2009).
- 20) S. Sarkar, T. Maitra, R. Valenti, and T. Saha-Dasgupta, *Phys. Rev. Lett.* **102**, 216405 (2009).
- 21) R. Nanguneri and S. Y. Savrasov, *Phys. Rev. B* **86**, 085138 (2012).
- 22) X. Luo, Y. P. Sun, L. Hu, B. S. Wang, W. J. Lu, X. B. Zhu, Z. R. Yang, and W. H. Song, *J. Phys.: Condens. Matter* **21**, 436010 (2009).
- 23) Y. Nii, N. Abe, K. Taniguchi, and T. Arima, *Appl. Phys. Lett.* **100**, 051905 (2012).
- 24) Y. Motome and H. Tsunetsugu, *Phys. Rev. B* **70**, 184427 (2004).
- 25) O. Tchernyshyov, *Phys. Rev. Lett.* **93**, 157206 (2004).
- 26) D. I. Khomskii and T. Mizokawa, *Phys. Rev. Lett.* **94**, 156402 (2005).
- 27) B. T. Thole, P. Carra, F. Sette, and G. van der Laan, *Phys. Rev. Lett.* **68**, 1943 (1992).
- 28) P. Carra, B. T. Thole, M. Altarelli, and X. Wang, *Phys. Rev. Lett.* **70**, 694 (1993).
- 29) T. Yokoyama, T. Nakagawa, and Y. Takagi, *Int. Rev. Phys. Chem.* **27**, 449 (2008).
- 30) M. Abbate, H. Pen, M. T. Czyzyk, F. M. F. de Groot, J. C. Fuggle, Y. J. Ma, C. T. Chen, F. Sette, A. Fujimori, Y. Ueda, and K. Kosuge, *J. Electron Spectrosc. Relat. Phenom.* **62**, 185 (1993).
- 31) E. Goering, O. Müller, M. L. denBoer, and S. Horn, *Physica B* **194**, 1217 (1994).
- 32) J.-S. Kang, J. Hwang, D. H. Kim, E. Lee, W. C. Kim, C. S. Kim, S. Kwon, S. Lee, J.-Y. Kim, T. Ueno, M. Sawada, B. Kim, B. H. Kim, and B. I. Min, *Phys. Rev. B* **85**, 165136 (2012).
- 33) C. T. Chen, Y. U. Idzerda, H.-J. Lin, N. V. Smith, G. Meigs, E. Chaban, G. H. Ho, E. Pellegrin, and F. Sette, *Phys. Rev. Lett.* **75**, 152 (1995).
- 34) Y. Takeda, M. Kobayashi, T. Okane, T. Ohkochi, J. Okamoto, Y. Saitoh, K. Kobayashi, H. Yamagami, A. Fujimori, A. Tanaka, J. Okabayashi, M. Oshima, S. Ohya, P. N. Hai, and M. Tanaka, *Phys. Rev. Lett.* **100**, 247202 (2008).
- 35) Y. Teramura, A. Tanaka, and T. Jo, *J. Phys. Soc. Jpn.* **65**, 1053 (1996).
- 36) C. Piamonteze, P. Miedema, and F. M. F. de Groot, *Phys. Rev. B* **80**, 184410 (2009).
- 37) W. A. Harrison, *Electronic Structure and the Properties of Solids* (Dover, New York, 1989).
- 38) G. van der Laan, R. V. Chopdekar, Y. Suzuki, and E. Arenholz, *Phys. Rev. Lett.* **105**, 067405 (2010).